Communications Chemistry

https://doi.org/10.1038/s42004-026-01886-y

Article in Press

Identification of an αvβ3-targeting bicyclic peptide with atypical *nor*Arg-Gly-Asp sequence

Received: 4 August 2025

Accepted: 2 January 2026

Cite this article as: Yang, H., Pan, H., Ran, T. *et al.* Identification of an αvβ3-targeting bicyclic peptide with atypical *nor*Arg-Gly-Asp sequence. *Commun Chem* (2026). https://doi.org/10.1038/s42004-026-01886-y

Haijian Yang, Hui Pan, Ting Ran, Wenyan Dong, Wencong Pan, Jianhui Tan, Jingjing Sun, Roderich D. Süssmuth, Wu Su & Guiyang Yao

Identification of an αvβ3-targeting bicyclic peptide with atypical *nor*Arg-Gly-Asp sequence

Haijian Yang [a, #], Hui Pan [b, #], Ting Ran [c, #], Wenyan Dong [b], Wencong Pan [b], Jianhui Tan [b], Jingjing Sun [b,*], Roderich D. Süssmuth [d,*], Wu Su [b, *] and Guiyang Yao [a,b, *]

[a]*School of Life Sciences, Fudan University, Shanghai 200438, China.*

[b]*Center for Innovative Drug Discovery, Greater Bay Area Institute of Precision Medicine (Guangzhou), Guangzhou 510000, China.*

[c] *Division of drug and vaccine research, Guangzhou National Laboratory, Guangzhou, 510005, China.*

[d]*Institut für Chemie, Technische Universität Berlin, Strasse des 17. Juni 124, 10623 Berlin, Germany.*

∗*Corresponding author: Jingjing Sun, E-mail: sunjingjing @ipm-gba.org.cn; Wu Su, E-mail: suwu@ipm-gba.org.cn; Roderich D. Süssmuth, Email: suessmuth@chem.tu-berlin.de; Guiyang Yao, E-mail: yaoguiyang@ipm-gba.org.cn.*

[#] *H.Y., H.P. and T.R. contributed equally to this work.*

Abstract: Bicyclic peptides, which integrate the advantageous properties of small molecules and antibodies, have emerged as a promising class of therapeutic candidates. In particular, integrin αvβ3 serves as a critical molecular target for cancer diagnosis and therapy. However, the development of bicyclic peptide ligands specifically targeting this integrin remains inadequately explored. To address this gap, we designed and synthesized a series of RGD-containing bicyclic peptides featuring a tryptathionine bridge. Notably, bicyclic peptide **5j** incorporates the non-canonical sequence *nor*Arg-Gly-Asp, exhibiting high affinity and selectivity toward integrin αvβ3. Molecular dynamics simulations provided insights into the conformational preferences and demonstrated that *nor*Arg plays a critical role in determining the selectivity between αvβ3 and αIIbβ3. Employing peptide **5j** as the targeting ligand, the peptide drug conjugates **P1** showed significant inhibitory effects on the A549 cell line in both, in vitro and in vivo experiments. These data provide important theoretical foundations for the development of αvβ3-targeting bicyclic peptides and offer new options for αvβ3-targeted tumor therapy.

Keywords: Bicyclic peptide, Integrin, Peptide drug conjugates, MD simulation, Anti-tumor activity

Introduction

Bicyclic peptides are a new modality that have the potential to become part of the next generation of therapeutics, combining specificity, potency, and attractive drug-like properties [1-5]. Their molecular structure is characterized by the incorporation of a constrained motif, which serves to restrict rotational freedom, thus locking the polypeptide chain into a more defined, rigid bicyclic conformation [6,7]. This structural attribute markedly diminishes the entropy penalties incurred during the interaction with biological targets, which in turn significantly enhances the affinity and selectivity of these peptides for challenging targets [3,8].

Integrin αvβ3 serves as a pivotal target in tumor-targeted therapy, renowned for its interaction with extracellular matrix (ECM) proteins containing the Arg-Gly-Asp (RGD) tripeptide sequence [9-13]. This interaction activates critical cellular signaling pathways, such as PI3K/Akt and FAK-MAPK2-4, which play essential roles in tumor growth and progression [11,14,15]. Cilengitide, the most advanced inhibitor targeting αvβ3[16,17], however exhibits pro-angiogenic and tumor-promoting effects at concentrations below its half-maximal inhibitory concentration (IC_{50}), which not only led to its failure in Phase III clinical trials for glioblastoma but also raised significant concerns about the development of integrin αvβ3-targeted therapeutics[18,19]. Although αvβ3 as an inhibitory target still presents certain limitations, recent studies have highlighted the regrowing interest in its application as a target for payload delivery in the field of tumor-targeted therapy[11,20,21]. Furthermore, a variety of probes for tumor imaging have been extensively developed employing RGD-based strategies targeting αvβ3 integrin and utilizing radionuclides, such as ^{18}F, ^{64}Cu, ^{68}Ga and ^{99m}Tc [22-28]. Notably, two related drug conjugates BGC0222 and VIP236 have advanced to clinical trial phases, thereby providing strong evidence for the translational potential of this target in precision oncology research[29,30].

In response to this pressing need, several cyclic peptides containing novel architectures[31-33], particularly bicyclic peptides targeting αvβ3, have been successively reported in the literature[24,34]. As early as 1995, Ruoslahti and co-workers utilized phage display to identify a bicyclic peptide named RGD4C, which is stabilized by two pairs of disulfide bonds and serves to constrain the spatial conformation of the peptide (see **Figure 1a**). Compared to the monocyclic peptide with a single pair of disulfide bonds and the RGD-containing linear peptide, RGD4C exhibited at least a 20-fold to 200-fold increase in inhibitory activity against cell binding to vitronectin, which emphasizes the importance of conformational restriction[35]. However, instability of the RGD4C disulfide bonds under reducing conditions is a potential disadvantage that can significantly reduce αvβ3 binding affinity[36,37]. In 2019, Timmerman and co-workers successfully identified a bicyclic peptide with exceptional selectivity for the αvβ3 integrin by leveraging the CLIPS peptide platform and incorporating the "1,3,5-tris(bromomethyl)benzene" constraint motif (see **Figure 1b**)[38,39]. It can thus be concluded that the design of bicyclic peptides by means of some high-stability

scaffolds is capable of preserving the selectivity of the designed molecules for integrin αvβ3 whilst simultaneously enhancing their inhibitory activity.

In this contribution we propose, that incorporating a tryptathionine bridge, which links the cysteine thiol group to the C-2 position of tryptophan, could serve as a novel constrained motif for the discovery of αvβ3-targeting bicyclic peptides (see **Figure 1c**). This modification is expected to enhance conformational rigidity and improve binding affinity, thereby facilitating the identification of αvβ3-targeting bicyclic peptides and potentially reshaping the landscape of cancer treatment.

To validate our hypothesis, we herein report a series of tryptathionine-bridged bicyclic peptides. By employing an ELISA integrin-extracellular matrix binding assay[40], we systematically optimized their structures and identified bicyclic peptide **5j**, which exhibits high affinity and selectivity for αvβ3 (IC_{50} = 0.7 ± 0.1 nM). Molecular dynamics simulations revealed the unique binding mode of this class of bicyclic peptides. Both in vitro and in vivo experiments comprehensively confirmed the ability of peptide **5j** to precisely target αvβ3, as well as its potential application value in the field of peptide-drug conjugates. Overall, our research provides significant insights into the development of αvβ3-targeting bicyclic peptides and expands the toolbox for precision targeting of tumors with elevated αvβ3 expression.

Results and Discussion

Molecular design, synthesis and integrin affinity of bicyclic peptides.

As a basic molecular design we grafted the conserved RGD motif, known for its targeting specificity to integrins, to the skeleton of the bicyclic cyclooctapeptide amanitin[41]. While the tryptathionine-cross-link was kept constant in order to stabilize the conformation, the original DHIle-HPro-Asn motif of the A ring was simplified to Ala-Pro-Asn, whereas the B ring was intended to carry the RGD motif. In the subsequent synthesis of an 11-membered peptide library we allowed for ring contractions, ring expansions and amino acid exchanges of the RGD motif [42]. Compounds **5a**-**5k** were synthesized using Fmoc-protected solid-phase peptide synthesis (SPPS), following the procedures outlined in **Scheme 1.**

The inhibitory activity of these peptides towards six integrins (α5β1, αvβ3, αvβ5, αvβ6, αIIbβ3, and αvβ8) was assessed employing an ELISA with integrin-extracellular matrix competing experiments (see **Table 1**). As reference compounds we used Kessler's *c*(RGDyK) (**6**) and the cyclic disulphide-bridged heptapeptide Eptifibatide (**7**) with specificities for αvβ3 and αIIβ3, respectively[40,43-47]. The experimental results showed that our prototypic bicyclic compound **5a** already exhibited potent inhibitory against αvβ3 (IC_{50} < 0.51 nM) while also demonstrating significant inhibitory activity against αvβ5 and αIIbβ3 (IC_{50} = 13.2 ± 1.2 nM and 1.9 ± 0.3 nM) respectively. Notably, the contraction to a seven-membered ring in **5b** did not enhance the selectivity of the bicyclic peptide for αvβ3 and αIIbβ3 integrins; instead, it resulted in a

decrease in inhibitory activity toward αvβ3 (IC_{50} = 7.8 ± 0.4 nM). To further optimize both, specificity and inhibition, we embarked on swapping of the Cys/Trp positions and rearranging the amino acid sequence (Asn-Pro-Ala) within the A ring of the bicyclic peptide, leading to the synthesis of compounds **5c** and **5d**. As the results demonstrate, compound **5c** displayed inhibitory activity against both αvβ3 and αIIbβ3 integrins, comparable to that of compound **5a**. In contrast, peptide **5d** also exhibited significantly enhanced selectivity for these two integrins while maintaining favorable affinity for αvβ3. These results underscore the importance of amino acids adjacent to the RGD sequence in modulating the selectivity of the bicyclic peptide ligands for integrins, in addition to the direct interaction with the RGD motif. Subsequently, in order to decrease the conformational rigidity of the peptides, we further modulated the bicyclic core structure by slightly increasing the individual ring sizes of the tryptathionine bridge (homoCys; **5e**) and of the macrolactam (β-Ala; **5f** and γ-aminobutyric acid (GABA); **5g**). However, these modifications led to a marked reduction in inhibitory towards all six integrins, aligning with the literature's assertion that a more rigid conformation typically enhances the ligand-receptor affinity[48]. Subsequently, we synthesized the bicyclic peptide **5h** incorporating D-Cys in the tryptathionine motif, however, no significant improvement in its inhibitory activity for αvβ3 was observed. These findings collectively contribute to an understanding of the structural parameters that govern the binding efficacy and specificity of bicyclic peptide ligands to integrins.

Based on a "spatial screening", Kessler and colleagues have elucidated that in the extended state of the RGD motif, an interatomic distance of 0.7-0.9 nm between the positively charged guanidinium group of Arg and the carboxy group of Asp is in support of a higher affinity for αIIbβ3 integrin. In contrast, when the binding motif adopts a more bent conformation, the ligand exhibits enhanced affinity for other integrin subtypes, such as αvβ3 and α5β1[49,50]. Hence, manipulating the spatial separation between the guanidinium group of the RGD motif and the carboxy group of Asp can be a critical factor in modulating the binding affinity for distinct integrin, specifically αvβ3 and αIIbβ3. To explore this modulation further, we designed and synthesized two bicyclic peptides, **5i** and **5j**. Peptide **5i** bearing L-*homo*Arg maintained its inhibitory activity towards αIIbβ3 (Table 1) compared to **5d**. Notably, this modification resulted in a marked reduction in its inhibitory activity against αvβ3 as well as the other four integrin subtypes. In contrast, the incorporation of L-*nor*Arg into peptide **5j** led to a minimal change in its inhibitory activity towards αvβ3 but induced a decrease in its inhibitory capacity for αIIbβ3. In order to obtain an idea on the impact of bicyclic peptides versus monocyclic peptides on the inhibitory activity, we synthesized **5k**. Interestingly, this peptide exhibited notable activity towards integrins αvβ3, αvβ5, and αIIbβ3, with half-maximal inhibitory concentrations (IC_{50}) of 0.3 ± 0.003 nM, 2.2 ± 0.2 nM, and 2.9 ± 0.4 nM, respectively. However, it did not show improved selectivity among these tested integrin subtypes. Accordingly, these results support that a bicyclic conformation is vital to the selectivity and affinity of binding αvβ3.

Summarizing the above results from integrin inhibition, the eight-membered bicyclic peptide **5j** was found to possess distinct advantages in terms of both, inhibitory activity and selectivity for the αvβ3 integrin. Furthermore, as a novel bicyclic peptide scaffold, **5j** exhibited binding characteristics that are comparable or even superior to those of the previously described αvβ3-targeting monocyclic peptide, *c*(RGDyK) (**6**). Notably, the affinity of **5j** for αvβ3, with an IC_{50} value of 0.7 ± 0.1 nM, is in the same range as that of cilengitide, a well-known αvβ3 inhibitor, which has an IC_{50} of 0.61 ± 0.06 nM [40]. This suggests that **5j** may serve as a promising candidate for further development in the realm of integrin-targeting therapeutics.

Molecular Docking

To further elucidate the influence of the guanidinium group on integrin binding activity, molecular docking (MD) studies were performed. Specifically, compound **5j** was docked with the RGD binding sites of the αvβ3 (PDB: 1L5G) and αIIbβ3 (PDB: 8T2U) followed by binding pose optimization using MD simulations (see **SI Methods**). According to the modeling results, compound **5j** interacts with both αvβ3 and αIIbβ3 in a similar manner, primarily by chelating the metal cation at the metal-ion-dependent adhesion site (MIDAS) via its Asp carboxylate group (see **Figure 2c** and **2d**). Additionally, the guanidinium group of **5j** forms a cation-π interaction with the phenyl ring of Y178 in αvβ3 and F160 in αIIbβ3. A key distinction is that **5j** forms a bidentate salt bridge with D218 in αvβ3 via its guanidino group, whereas this interaction is absent in its binding to αIIbβ3. In αIIbβ3, an acidic residue, D224, is located distally from the guanidinium group of **5j**. However, in compound **5i**, which possesses a longer homoarginine side chain, a salt bridge with D224 may be formed, potentially explaining its higher activity against αIIbβ3 compared to **5j**. Furthermore, differences in hydrogen bonding patterns are observed in the interactions with αvβ3 and αIIbβ3. The backbone amide and carbonyl groups of the tryptophan moiety in **5j** form two hydrogen bonds with D251 and N313 of integrin β3, respectively (see **Figure 2c**). In its interaction with αIIbβ3, only the hydrogen bond with N313 is present. Nonetheless, the additional hydrogen bonds formed around the MIDAS site may compensate for this (see **Figure 2d**), suggesting that variations in hydrogen bonding are unlikely to be the primary factor driving the high selectivity of **5j** for αvβ3 over αIIbβ3. Overall, the unique interaction pattern of the guanidinium group of nor-Arg within the RGD binding domain of αvβ3 likely contributes to the nanomolar IC_{50} of **5j**, reinforcing its potent and selective binding affinity (see **Figure 2a-2b**). Similarly, from our library another selective αvβ3 inhibitor **5d**, exhibits a comparable difference in the binding mode between the two integrins (see **Figure S2**).

Cy5-labeled compound 5j-K-Cy5 specifically binds integrin αvβ3 and is internalized by MDA-MB-231 cells.

To evaluate the binding and uptake capabilities of the bicyclic peptide **5j** on αvβ3-expressing cells, we labelled the peptide structure with the fluorescent dye Cy5. Since **5j** inherently lacks additional conjugation sites, we replaced alanine (Ala) in **5j** with an orthogonally protected lysine (Lys(Dde)), which facilitates the synthetic attachment of Cy5 in the sidechain. In contrast, Asp/Asn as an alternative attachment site is not ideal due to its unique capacity to be involved in turn structures (Asx turn) [51,52]. Molecular dynamics simulations reveal that the side-chain amide bond of Asn in **5j** participates in intramolecular hydrogen bonding (see **Figure 2d**), which most likely contributes to maintaining the spatial conformation of the bicyclic peptide. Along these lines Cy5-labeled **5j-K-Cy5** and **6-Cy5** (a validated αvβ3 ligand for tumor imaging/drug delivery as positive control[22,43,44,53,54]) were synthesized (**Scheme S1**), together with **A20FMDV-Cy5** (specific to αvβ6; αvβ3-negative control) to evaluate target specificity of **5j**[55].

Three cell lines - MDA-MB-231 (17.03% αvβ3), A549 (13.60% αvβ3), and Huh-7 (<0.7% αvβ3/αvβ6) - were selected based on CCLE database analysis for functional assays. Flow cytometry validation (see **Figure 3a** and **Figure S3**) confirmed MDA-MB-231 as suitable αvβ3-positive and Huh-7 as an αvβ3-negative control cell lines, with αvβ6 expression consistently ≤0.7% across all three cell lines. The results of the cell binding experiments are shown in **Fig. 3b**, where red fluorescence indicates the Cy5 signal, and the blue fluorescence corresponds to the DAPI-stained nuclei. Following incubation with Cy5-labeled peptides at 4 °C for 1 h, significant binding of **5j-K-Cy5** to αvβ3-positive cells was observed. Similarly, the positive control compound **S6-Cy5** exhibited comparable binding signals. In contrast, **A20FMDV-Cy5**, a peptide specifically binding to αvβ6, displayed negligible fluorescence signals on MDA-MB-231 cells. For Huh-7 cells, which are negative for both αvβ3 and αvβ6 expression, no significant signals were observed for any of the three Cy5-labeled peptides. These results confirm that the designed and synthesized bicyclic peptide **5j** exhibits specific binding to integrin αvβ3.

To verify whether the bicyclic peptide **5j** could serve as a targeting peptide for drug delivery in the treatment of tumors with high αvβ3 expression, we conducted cellular uptake and lysosome co-localization experiments using MDA-MB-231 cells (see **Figure 3c**). Following co-incubation of Cy5-labeled peptides with cells at 37°C for 4 h, analysis by confocal fluorescence microscopy demonstrated that the peptide **5j-K-Cy5** exhibited a marked enhancement in cellular internalization when compared to the reference compound **6-Cy5**. Additionally, the Cy5 fluorescence signal displayed a high degree of co-localization with the green fluorescence signal of LAMP1 (see **Figure 3d**), a validated lysosomal marker, indicating that **5j-K-Cy5** is indeed internalized by the cells via the lysosomal pathway. Since cathepsin B is highly expressed in the lysosomal environment, it is capable of efficiently cleaving the peptide-payload conjugates, thereby facilitating the release of therapeutic compounds within target cells [56-58]. These cumulative observations not only demonstrate the effective internalization and processing of **5j-K-Cy5** within lysosomes but also

provide robust support for the strategic use of αvβ3-targeted peptide-drug conjugates (PDCs) as a modality for tumor-specific drug delivery.

Evaluation of the cytotoxicity of αvβ3-selective peptide-toxin conjugates against CCK-8 cell lines.

Before conducting the experiment, the *in vitro* plasma stability of the side chain-deprotected bicyclic peptide **5j-K** was evaluated. The results demonstrated that the tested bicyclic peptide exhibited sufficient stability in rat plasma ($t_{1/2}$ > 11 h, see **Figure S1**). Then, the microtubule inhibitor monomethyl auristatin E (MMAE) was selected as the toxin payload, due to the presence of extensive data on both, antibody drug conjugates (ADCs) and peptide-drug conjugates (PDCs)[59,60]. Accordingly, four peptide toxin conjugates (PTCs), namely **P1**, **P2**, **P3**, and **P4**, were synthesized according to methods outlined in **Scheme S4-6** (see **Figure 4a**). All four conjugates incorporate the 6-azidohexanamido-VA-PABC-MMAE linker-drug module, which was conjugated to the peptide via a copper-catalyzed azide-alkyne cycloaddition (CuAAC) reaction. Compounds **P1** and **P2** utilize **5j-K** as the integrin-targeting peptide, whereas **P3** employs deprotected compound **8** (non-binding AGD motif) as the negative control, and compound **P4** utilizes compound **6** (*c*(RGDyK)) as the positive control. Compounds **P1, P3** and **P4** feature an octaethylene glycol (PEG_8) spacer, while **P2** utilizes a C_8 aliphatic chain as a spacer. Subsequently, the cytotoxicity of the four conjugates against the human tri-negative breast cancer cell line MDA-MB-231 and the human non-small-cell lung cancer cell line A549[44] was evaluated using a standard CCK-8 cell viability assay (see **Table 2, Figure S4a and S4b**). Following a 72 h incubation, the CCK-8 assay results showed that the naked peptides **6** and **5j-K** had no significant toxic effects (IC_{50} > 5 μM), whereas the drug MMAE alone exhibited potent cytotoxicity (IC_{50} < 1.37 nM). The positive control **P4** demonstrated IC_{50} values of 58.5 ± 3.9 nM in MDA-MB-231 cells and 37.9 ± 8.4 nM in A549 cells. Both **P1** and **P2** exhibited enhanced efficacy relative to **P4**, with IC_{50} values in MDA-MB-231 cells of 41.3 ± 4.1 nM and 31.23 ± 4.3 nM, respectively, and in A549 cells, of 31.3 ± 4.3 nM and 18.5 ± 4.0 nM. The negative control **P3** exhibited comparatively lower anti-proliferative activity, with IC_{50} values of 72.2 ± 7.9 nM in MDA-MB-231 cells and 94.1 ± 25.9 nM in A549 cells.

Meanwhile, we knocked down the mRNA associated with αvβ3 expression in A549 cells (A549-KD (αvβ3-)) through transient transfection and verified the successful knockdown of αvβ3 protein via Western blot (see **Figure S4e**). In parallel, A549 cells treated with a non-targeting scrambled siRNA (si-NC) were used as the control (A549-si-NC ($\alpha v\beta 3^{+}$)). Subsequently, in vitro cell proliferation inhibition experiments demonstrated that, for all three conjugates, the IC_{50} value in A549-KD (αvβ3-) cells increased by about 2-fold compared to A549-si-NC (αvβ3+) cells (see **Table 3**). The IC_{50} of **5j-K** conjugates **P1** and **P2** in A549-KD (αvβ3-) was 1.6-fold and 1.9-fold higher than A549-si-NC (αvβ3+), while for the positive control *c*(RGDyK) conjugate **P4**, the IC_{50} was 1.7-fold higher. These findings indicate that **P1** and **P4**, to some

extent, enhance cellular internalization and cytotoxicity through specific recognition of αvβ3 by peptide **5j-K** and *c*(RGDyK).

To further elucidate the importance of targeted peptides and assess the binding capability of conjugates to integrin receptors on cell surfaces, we performed a "kiss and run" experiment [61,62]. The results demonstrate that conjugate **P1** exhibited greater antiproliferative activity than the negative-control conjugate **P3** (see **Table S1**). Moreover, the relative potency (RP) of the conjugates in the two tested cell lines correlates well with αvβ3 integrin expression levels, thereby confirming the specific targeting ability of bicyclic peptide **5j** toward αvβ3 integrin. These findings indicate that the conjugations of MMAE to the peptide substantially reduces its cytotoxicity, likely as a result of decreased non-specific cellular uptake of MMAE. While **P1** and **P2** did not exhibit a marked difference in cytotoxicity compared to **P4**, their significant inhibitory capacity underscores the therapeutic potential of PDCs utilizing the **5j-K** peptide as a targeting-αvβ3 ligand for tumor therapy.

In vivo antitumor activity of peptide-toxin conjugates.

To assess the *in vivo* antitumor activity of the PTCs, we employed an A549 xenograft mouse model (BALB/c) for efficacy studies. In preliminary CCK-8 cellular assays, **P2** exhibited stronger proliferation inhibition compared to **10a**. However, the solubility of **P2** in a 10% DMSO-PBS solution was compromised owing to the presence of a lipid chain, leading us to select **P1** for the *in vivo* antitumor efficacy assessment. We first evaluated two doses of **P1** (2 mg kg^{-1} and 0.5 mg kg^{-1}) against a control group receiving 10% DMSO in PBS (pH 7.4) (n=6 per group). Treatment initiation occurred when tumors reached a volume of 100-150 mm^3, with intravenous tail vein injections administered biologically. Tumor volume and mouse body weight were monitored prior to each injection. Notably, mice in the 2.0 mg kg^{-1} dose group exhibited a decrease in body weight by the third day post-administration, which intensified by the fifth and seventh days, culminating in mortality. This indicated that the 2.0 mg kg^{-1} dose was excessively high and inappropriate for continued in vivo experimentation (see **Figure S5b-c**). In contrast, the 0.5 mg kg^{-1} dose group displayed minimal to no significant change in body weight, and even showed a slight increase, relative to the PBS control group. Moreover, this lower dose effectively suppressed tumor growth, with a significantly reduced tumor growth rate compared to the control ($p < 0.05$) (see Figure **S5b-d**).

To further delineate the *in vivo* antitumor efficacy and targeting specificity of **P1**, we conducted a long-term study using a 1.0 mg kg^{-1} dose of **P1** and an equimolar dose of MMAE (0.29 mg kg^{-1}), with the 10% DMSO PBS solution serving as a control (n=7 per group). Over the course of a 21-day treatment regimen, mice administered with **P1** showed no significant weight loss or side effects, in marked contrast to those receiving an equimolar dose of MMAE (see **Figure 4a-d**). The tumor size in the group treated with 1.0 mg kg^{-1} **P1** was significantly controlled ($p < 0.001$) compared to the vehicle control group. There was also no

significant difference in liver and kidney functions between 1.0 mg kg^{-1} **P1** and the vehicle control group (see **Figure 4f**). Tissue distribution studies demonstrated significant enrichment of the payload drug MMAE in tumors 4 h after administration (see **Figure S7**). Moreover, IHC staining of Ki67 indicated a significantly reduced tumor proliferation in the treatment group (see **Figure 4g**). Although the MMAE control group displayed comparable inhibitory effects early in the treatment, prolonged exposure resulted in significant weight loss, indicating high toxicity. These findings suggest that **P1** is an effective inhibitor of αvβ3-positive tumor growth in the mouse xenograft model, with reduced side effects compared to free MMAE. Finally, we assessed the antitumor activity of conjugate **P4** with the targeting peptide *c*(RGDyK) in A549 tumor-bearing mice (n = 6). Over the course of a 21-day treatment regimen, mice administered with 0.9 mg kg^{-1} **P4** showed no significant weight loss or side effects (see Figure **S6a-d**). The tumor progression in the group treated with 0.9 mg kg^{-1} **P4** was significantly suppressed ($p < 0.001$) compared to the vehicle control group, but the antitumor effect is not superior to that of an equivalent amount of **P1**. The tumor growth inhibition (TGI) results indicate that **P1** exhibits a comparable yet slightly superior tumor-suppressive effect. These results underscore the specific targeting efficacy of the bicyclic peptide **5j** to αvβ3 integrin and reinforce its potential value as an αvβ3-targeting ligand for drug delivery in tumor therapy.

Conclusion

In conclusion, our study has characterized a novel bicyclic peptide **5j**, which exhibits high affinity and specificity for the integrin αvβ3 receptor. The molecular structure of **5j** incorporates the non-canonical sequence *nor*Arg-Gly-Asp, which serves as a critical determinant in its discriminative selectivity towards αvβ3 over the αIIbβ3. In light of the molecule's capability to be internalized by cells via the endosome-lysosome pathway, we have successfully synthesized two peptide-drug conjugates, **P1** and **P2**. Our in vivo evaluation using a mouse tumor xenograft model has demonstrated that **P1** induced potent tumor suppression effects while significantly reducing systemic side effects compared to free MMAE alone. This comparative efficacy and safety profiles highlight the advantages of our targeted peptide-drug conjugate strategy. The findings of this research not only validate the therapeutic potential of **5j** as a novel bicyclic peptide for αvβ3-targeted tumor therapy but also provide critical theoretical and practical insights into the development of αvβ3-targeting bicyclic peptides.

Methods

Chemistry

Chemical materials

The analytical reagents were purchased from Energy Chemical and Fisher without further purification. 2-CTC resin, TBTU, HATU, and Fmoc-protected amino acids were purchased from Bide Pharmatech Ltd., DIEA, TFA, and HFIP were purchased from MACKLIN. Purity (>95%) confirming and reaction

monitoring were carried out on analytical UHPLC (ThermoFisher Scientific Vanquish.) using an ODS column (Welch Ultimate UHPLC XB-C18 column, 2.1 mm × 100 mm, 1.8 μm). Final compounds were purified on preparative HPLC SHIMADZU LC-20AP using an ODS column (Welch Ultimate AQ-C18 column, 21.2 mm × 250 mm, 5 μm). HR ESI–MS data were acquired using LCMS (HPLC SHIMADZU LC-40D, MS Sciex ZenoT0FTM 7600, Column Synergi^{TM} 4 μm Fusion-RP 50 × 2 mm). ^{1}H NMR spectra were recorded by Bruker Advance (400 MHz) using TMS as an internal Standard and DMSO-d_6 as solvents, and the chemical shift was reported in parts per million (ppm). Purity assessment of synthesized compounds was performed using HPLC, NMR (see Supplementary Information and Supplementary Data 3).

The synthesis of Cy5-labeled peptides

The Dde-group-deprotected peptide **S3** (15 mg, 0.01 mmol) was dissolved in DMF (5 mL), and Cy5-sulfo (7.9 mg, 0.012 mmol) was conjugated using the coupling agent HATU (2.0 eq). After reacting at room temperature for 2.0 hours, the DMF solvent was removed by rotary evaporation (See SI **Scheme S1**). Then a mixed solvent of TFA/TIS/H_2O (95:2.5:2.5) was added to remove the remaining sidechain protecting groups at room temperature for 0.5 h. The product was precipitated with ether and purified to obtain the Cy5-labeled compound **5j-K-Cy5** as a blue solid 10.6 mg for 67.3% yield (purity > 96%). **HR ESI–MS:** exact m/z calculated for $C_{73}H_{95}N_{16}O_{18}S_3^+$ $[M+H]^+$ = 1579.6167, found 1579.6125 (see **Figure S14**).

Following the general protocol for solid-phase peptide synthesis, a side-chain fully protected peptide was synthesized via solid-phase peptide synthesis. Subsequently, the Dde group was removed by treating the peptide with 2% hydrazine hydrate in DMF for 10 minutes at room temperature (r.t.). The mixture was then concentrated and purified by preparative HPLC to afford the target product **S1** as a white solid. Next, the same method was employed to get the compound **6-Cy5** as a blue solid 7.7 mg (See SI **Scheme S1**) for 61.2% yield (purity > 96%). **HR ESI–MS:** exact m/z calculated for $C_{60}H_{80}N_{11}O_{15}S_2^+$ $[M+H]^+$ = 1258.5271, found 1258.5216 (see **Figure S12**).

The synthesis of peptide-toxin conjugates P1, P2, P3 and P4

Fmoc-L-Lys(Dde)-OH was used to replace Fmoc-L-Ala-OH in compound **5j**. Following the general protocol provided in the Supporting Information, a side-chain fully protected bicyclic peptide was synthesized via solid-phase peptide synthesis. Subsequently, the Dde group was removed by treating the peptide with 2% hydrazine hydrate in DMF for 10 minutes at room temperature (r.t.). The mixture was then concentrated and purified by preparative HPLC to afford the target product as a white solid. Next, the Dde-group-deprotected peptide **S3** (30 mg, 0.02 mmol) was dissolved in DMF (5 mL), followed by the addition of Propargyl-PEG8-acid (**S10**, 1.5 equiv), HATU (2.0 equiv), and DIPEA (2.2 equiv). The reaction mixture was stirred at rt for 2 hours. Afterward, the DMF was removed under reduced pressure, and the crude product was treated with a mixture of TFA/TIS/H_2O (95:2.5:2.5, v/v) at rt for 0.5 hours. Following concentration, ether (30 mL) was added to precipitate the product, which was subsequently collected by

centrifugation. Subsequently, the precipitate was redissolved in DMF/H_2O (2:1, v/v). Then, 6-azidohexanamido-VA-PABC-MMAE **S9** (35.5 mg, 0.03 mmol), $CuSO_4 \cdot 5H_2O$ (20 mg, 0.08 mmol), and sodium ascorbate (31.7 mg, 0.16 mmol) were added sequentially. The reaction mixture was stirred at room temperature (r.t.) for 1 hour. The crude product was subsequently purified by preparative HPLC and then lyophilized to afford the final desired product **P1** as a white powder with a yield of 40.2mg (79.3%). and a purity of 98%. **HR ESI–MS:** exact *m/z* calculated for $C_{121}H_{188}N_{25}O_{32}S^+$ $(M + H)^+$: 2535.3567, found 2535.3541 (see SI **Scheme S3, Figure S17-18)**.

The synthesis procedure of **P2-P4** follows a methodology similar to that described previously. For detailed experimental conditions and synthetic parameters, the reader is referred to the supporting literature (See **Scheme S4-S6**)

Biological assays

Materials:

Dulbecco's phosphate-buffered saline (DPBS, pH 7.4), phosphate-buffered saline (PBS, pH 7.4), DMEM basic (1×), DMEM/F-12 (1:1) basic (1×), fetal bovine serum (FBS), and trypsin/EDTA were obtained from Gibco™. ECM proteins (extracellular matrix proteins: Recombinant Human Vitronectin Protein, catalog no. 2308-VN-050; Recombinant Human LAP (TGF-beta 1) Protein, catalog no. 246-LP-025; Recombinant Human fibronectin, catalog no. 4305-FNB-200), human integrin proteins (Recombinant Human Integrin αvβ3, catalog no. 3050-AV-050; Recombinant Human Integrin αvβ5, catalog no. 2528-AV-050; Recombinant Human Integrin αvβ6, catalog no. 3817-AV-050; Recombinant Human Integrin αvβ8, catalog no. 4135-AV-050; Recombinant Human Integrin αIIbβ3, catalog no. 7148-A2-025; Recombinant Human Integrin α5β1, catalog no. 3230-A5B-050), detection antibodies (Human Integrin alpha V/CD51 Biotinylated Antibody, catalog no. BAF1219; Human Integrin beta 3/CD61 Biotinylated Antibody, catalog no. BAF2266; Human Integrin beta 1/CD29 Biotinylated Antibody, BAF1778) and Streptavidin-HRP (catalog no. DY998) were purchased from R&D. Cell counting kit-8 (CCK-8, catalog no. C0039) and 4,6-diamidino-2-phenylindole DAPI (catalog no. C1002) were obtained from Beyotime. Anti-LAMP1 antibody (catalog no. ab278043) was purchased from Abcam. Cy3-conjugated AffiniPure™ Goat Anti-Rabbit IgG (H+L) (minimal cross-reaction to Human, Mouse, and Rat Serum Proteins) was purchased from Jackson (catalog no. 111-165-144). Ki67 Cell Proliferation Kit (IHC) (catalog no. E607235-0100) was obtained from Sangon Biotech (Shanghai, China). DMSO (>99.9%, HPLC) was purchased from MACKLIN. All aqueous solutions were prepared using Milli-Q purified water (18.2 MΩ). Flat bottom 96 well cell culture plates were purchased from Corning Incorporated Costar. Human breast cancer cell line MDA-MB-231, human hepatoma cell line Huh-7 cells and human lung carcinoma cell line A549 cells were initially purchased from the Chinese Academy of Science Shanghai Institute of Cell Bank

(Shanghai, China). Male nude mice (SPF, 5-6 weeks) were purchased from GemPharmatech (Guangdong, China). The absorption was recorded by microplate spectrophotometer (TECAN, Infinite E Plex). Confocal fluorescence imaging was performed using the confocal laser scanning microscope (Leica STELLARIS). The biochemical indicators (ALT, AST and UREA) testing was performed on a fully automated biochemical analyzer (mindray, BS-240VET).

Integrin Binding Assay

The activity and selectivity of cyclic peptide integrin ligands were assessed through an integrin-extracellular matrix interaction assay based on ELISA detection, following the previously reported method[40]. Using **6** *c*(RGDyK) as a reference reagent, other reagents including ECM proteins, human integrin proteins, detection antibodies. Initially, ECM proteins were dissolved in carbonate buffer (15 mM Na_2CO_3, 35 mM $NaHCO_3$, pH 9.6), then added to a flat-bottom 96-well plate at 100 μL per well, incubated overnight at 4°C. The plate was then washed with PBS-T buffer (phosphate-buffered saline/Tween20, 137 mM NaCl, 2.7 mM KCl, 10 mM Na_2HPO_4, 2 mM KH_2PO_4, 0.01% Tween20, pH 7.4; 3 × 200 μL), followed by blocking with TSB buffer (Tris-saline/BSA buffer, 150 μL/well, 20 mM Tris-HCl, 150 mM NaCl, 1 mM $CaCl_2$, 1 mM $MgCl_2$, 1 mM $MnCl_2$, pH 7.5, 1% BSA) at room temperature for 1 h. Meanwhile, serial dilutions of the reference reagent and test compounds were prepared in a separated 96-well plate, starting from 1 μM and following a 3-fold gradient dilution across 10 concentration points. After washing the assay plate with PBS-T (200 μL) three times, 50 μL of each dilution was transferred to each well from B-G of the assay plate. Well A was filled with 100 μL of TSB solution as a blank, and well H was filled with 50 μL of TSB buffer. Then 50 μL of human integrin in TSB buffer was added to wells H-B, and the plate was incubated at room temperature for 1 h. The detection antibody was added after washing the plate with PBS-T buffer three times (100 μL per well). Following a 1 h incubation at room temperature, the plate was washed three times with PBS-T buffer. Then Streptavidin-HRP was then added (diluted 1:10, 100 μL per well) and incubated at room temperature for 1 h, after which the plate was washed three times with PBS-T buffer. Then the substrate SeramunBlau was quickly added to the plate (50 μL per well) and incubated in the dark for 5 min. Then 50 μL of 3 M H_2SO_4 stop solution was added to each well, and the absorbance was measured at 450 nm using a microplate reader (TECAN, Infinite E Plex). The IC_{50} for each compound was tested in duplicate and analyzed using Origin 2025 software.

Cell culture

MDA-MB-231 cells and Huh-7 cells were cultured in Dulbecco's Modified Eagle Medium (DMEM), and A549 cells were cultured in DMEM/F-12 (1:1). The medium was supplemented with 10% fetal bovine serum (FBS) and 1% penicillin streptomycin solution. The cells were grown in sterile cell culture flasks and maintained in 5% CO_2 in a humidified incubator at 37 °C.

Flow cytometry analysis for cell surface integrin proteins

MDA-MB-231, A549 and Huh-7 cells were added to each centrifuge tube at a density of 2×10^5 for αvβ3 determination and 5×10^5 for αvβ6 determination. Then, 1 mL buffer (2% FBS/98% DPBS) was added to disperse cells and centrifuged (400 × g, 5 min). After discarding the supernatant, antibody (αvβ3, catalog no. 304415, Biolegend; αvβ6, catalog no. FAB4155A, R&D) was added and incubated in the dark at 0 °C (αvβ3 for 20 min, αvβ6 for 40 min). Then cells were washed with pre-chilled buffer (2 mL) twice. Dead cells were stained with PE Annexin V Apoptosis Detection Kit I (catalog no. 51-68981E, BD) for 20 min. Finally, the assay was performed on a flow cytometer (CytoFLEX LX).

Confocal microscopy of Cy5-labeled peptides binding to αvβ3-expressing cells

MDA-MB-231 (1.8×10^4 cells per well) and Huh-7 (1.6×10^4 cells per well) cells were seeded in a flat-bottom 96-well plate with transparent glass bottoms and cultured in DMEM high glucose medium for 48 hours, respectively. After microscopic observation confirmed that the cells had reached an appropriate density, the culture plate was incubated at 4 ℃ for 20 minutes. Meanwhile, Cy5-labeled compounds **6-Cy5** and **5j-K-Cy5** were prepared as 5 μM test solutions in DMEM high-glucose medium and subsequently maintained in the dark at 4 ℃ for the same duration. After removing the old medium, the test solutions were added to the corresponding wells, then the cells were incubated with 5 μM of **6-Cy5** and **5j-K-Cy5** at 4 ℃ in the dark for 1 hour. Following incubation, the test solutions were removed, and the cells were carefully washed twice with pre-cooled PBS (1×). Subsequently, the cells were fixed with 4% paraformaldehyde solution at room temperature for 20 minutes. After discarding the fixative, the cells were washed twice with PBS (1×). Subsequently, 100 μL DAPI solution (1:5000) was added to each well to stain the nuclei at room temperature for 20 minutes. After washing twice with PBS (1×), 55 μL of DAPI-free antifade mounting medium was added to seal the plates. Finally, the plates were observed and imaged under an inverted confocal fluorescence microscope (Leica STELLARIS).

Confocal microscopy of internalization of Cy5-labeled peptides into the αvβ3-expressing cell

MDA-MB-231 cells (1.8×10^4 cells per well) were seeded in a flat-bottom 96-well plate with transparent glass bottoms and cultured in DMEM high glucose medium for 48 hours. After discarding the medium, the cells were incubated with 5 μM of pre-prepared Cy5-labeled peptide solutions in DMEM at room temperature for 4 hours. Subsequently, discarding the solutions, the cells were washed twice with PBS (1×), and the cells were fixed with 4% paraformaldehyde for 20 min. After that, washed twice and permeabilized with 0.15% Triton X-100 for 15 min. Then, the cells were blocked with 10% goat serum at room temperature for 1 hour and incubated with anti-LAMP1 primary antibody (1:300) at 4 ℃ in the dark overnight. After incubation, cells were returned to room temperature and washed three times with PBS. Next, Cy3-conjugated AffiniPure™ goat anti-rabbit (1:300) secondary antibody was incubated with the cells at room temperature for 1 hour. After washing, the nuclei were stained with (DAPI). Finally, the

fluorescence staining was observed and photographed with an inverted confocal microscope (Leica STELLARIS).

Measurement of cytotoxicity by CCK-8 assay

The toxicity determination CCK-8 experiment was carried in 96-well plates. MDA-MB-231 (3.0×10^3 cells per well) and A549 cells (3.0×10^3 cells per well) were seeded in 96-well plates and incubated for 24 h. Then the medium was discarded and treated with **5j-K**, **6**, **P1**, **P2, P3** or **P4** in various concentrations (5.0 μM, 2.5 μM, 1.0 μM, 333.33 nM, 111.13 nM, 37.04 nM, 12.35 nM, 4.12 nM, 1.37 nM) for another 72 h. Following with conventional CCK-8 treatment. After 1 h, the formazan dye was quantified using a microplate reader to assess absorbance at 450 nm (measurement wavelength) and 630 nm (reference wavelength). Non-treated cells were used as controls. The percentage viability of cells was estimated as the percentage fluorescence intensity in the experimental wells relative to that in the blank and negative control wells. Each experiment was repeated three times.

RNA interference for αvβ3 and cell viability detection

A549 cells were seeded in 96-well plates at a density of 500 cells per well and allowed to adhere overnight in high-glucose DMEM supplemented with 10% fetal bovine serum (FBS) without antibiotics. Small interfering RNAs (siRNAs) targeting human ITGAV (sequence: 5'-3' CCAUGUAGAUCACAAGAUAdTdT) and ITGB3 (sequence: 5'-3' GCUACAGUCUGUGAUGAAAdTdT) were used at 1.2 pmol per well each (total 2.4 pmol/well). A non-targeting siRNA negative control (siRNA NC, same dosage; GenScript Biotech Corporation, Order No. C717J577G0) served as the control. The siRNA mixtures were complexed with 0.2 μL/well Lipofectamine RNAiMAX Reagent (Invitrogen, REF: 13778100) in OPTI-MEM (Gibco, catalog no. 31985-062) and incubated at room temperature for 20 minutes before being added to the cells. At 6 hours post-transfection, the medium was replaced with high-glucose DMEM containing 10% FBS and 1% penicillin-streptomycin (P/S). Test drugs were administered at 48 hours post-transfection, and after 72 hours of co-incubation, cell viability was assessed using the CCK-8 assay (Beyotime, catalog no. C0039).

Western Blot Analysis for αvβ3 Knockdown Verification

Parallel plates of A549 cells transfected for 48 h were lysed with strong RIPA lysis buffer (Beyotime, Catalog No. P0013B). Proteins (30 μg) were separated by 4-12% SDS-PAGE (ACE Biotechnology, Cat. ET15412LGel) and transferred to PVDF membranes using 10× WB Transfer Buffer (Solarbio, Cat. No. D1060). Membranes were blocked with 5% skim milk in TBST (Servicebio, Cat: G0001-2L) for 2 h. Primary antibodies were diluted in Beyotime Western Primary Antibody Dilution Buffer (Beyotime, Catalog No. P0023A-500ml): rabbit anti-ITGB3 (ABclonal, A19073, 1:1000) or mouse anti-GAPDH (Santa Cruz, sc-32233, 1:2000), and membranes were incubated with these antibodies overnight at 4 °C.

Secondary antibodies (Invitrogen, 31460 or 31430, 1:5000) were diluted in Beyotime Western Secondary Antibody Dilution Buffer (Beyotime, Catalog No. P0023D-500ml) and incubated with membranes for 1.5 h at room temperature. Bands were visualized using Clarity™ Western ECL Substrate (Bio-Rad, Cat. #170-5061) and imaged with a Tanon 5200 imaging system. Band intensities were quantified using Gel-Pro Analyzer 4 software, and ITGB3 signal was normalized to GAPDH.

In vivo assay

All animal experiments were carried out using 6-week-old male nude mice weighing 20–25 g purchased from GemPharmatech (Guangdong, China). These mice were maintained in a specific pathogen-free environment with free access to water and food. Experiments were approved by the Ethics Committee for Animal Experimentation of Greater Bay Area Institute of Precision Medicine (Guangzhou) in compliance with relevant laws and institutional rules. To establish xenograft models, A549 cells were injected (1×10^7 cells/200 μL) into the right flank of athymic nude mice. Mice were randomly divided into groups (n = 6/7) after the tumors had reached a size of 100-150 mm^3. Drug solutions (100 μL each) were administered through the tail vein once every 2 days for a total of 10 injections (21 days): 2.0 mg kg^{-1}, 1.0 mg kg^{-1} and 0.5 mg kg^{-1} per injection of **P1**, 0.29 mg kg^{-1} per injection of MMAE, and PBS as a control. The body weights and tumor sizes of each mouse were measured before drug injections. And tumor volume was estimated using the following equation: TV (mm^3) = $d^2D/2$, where *d* and D are the shortest and the longest diameter, respectively[63]. Tumors were dissected, measured, and photographed on day 21 after mice were sacrificed by cervical dislocation. Cell proliferation was determined by immunohistory chemical staining of Ki67 according to the Ki67 Cell Proliferation Kit (IHC) (E607235, Sangon Biotech, China). Image acquisition was performed using Nikon ECLIPSE Ni-U microscopes with 40x objective. The percentage of Ki67 positive cells was analyzed by ImageJ (NIH). The biological activity of **P1** and the other substances was compared using one-way ANOVA. Statistical analyses were performed using Origin 2025. and $p < 0.05$ was considered significant. Error bars in the figures indicate standard deviations of the mean.

Plasma stability assay

Firstly, internal standard testosterone was chosen to be dissolved in ACN to be a concentration of 500 nM. Side chain-deprotected bicyclic peptide **5j-K** (1.51 mg) was dissolved in 1.4 mL of DMSO to be a stock solution, then 10 μL stock solution was diluted using 190 μL MeOH, then 2.5 μL dilution was added to rat plasma (pH 7.5) at 37 °C to give final concentration for bicyclic peptide of 1 μM. The plasma was incubated for 24 h at 37 °C and 600 rpm. At 0, 0.5, 1, 2, 4, 6, 8, and 24 h, 25 μL of plasma was withdrawn and precipitated with 50 μL of cold quenching solution consisting of ACN with a final concentration of 333 nM testosterone as an internal standard. The samples were stored at 4 °C and centrifuged (12000 g, 4 °C, 5 min). The supernatant was analyzed by LC−MS (injection volume, 5 μL). The degradation was determined by comparing the peak area of the MS signal of the internal standard with the tested compound. And the

percentage of the remaining amounts of **5j-K** at each time interval was calculated based on the 0 h of peak area.

Liver and kidney functions

Blood was collected from the mice before euthanasia, then centrifuged to obtain plasma for measuring biochemical indicators of liver and kidney function. The biochemical tests (ALT, AST, and UREA) were performed on a biochemical analyzer (Mindray, BS-240VET) using ALT Kit (IFCC method) (Mindray, Lot 140124026), AST Kit (IFCC method) (Mindray, Lot 140224024), and UREA Kit (Urease-GLDH, UV method) (Mindray, Lot 141325001), respectively.

Tissue distribution

For tissue distribution tests, xenografts with tumors in the flank were prepared as mentioned previously. The compound solution of **P1** (1 mg kg^{-1}) was administered into mice (n = 3) by intravenous tail vein injection (100 μL). Blood was collected after 4 h of injection, then the mice were euthanized, and the organs (tumor, brain, heart, liver, lung, kidney, stomach, and pancreas) were collected and kept in a deep freezer until further use. The weight of each dissected tissue was measured, and PBS at a ratio of 1:3 (tissue weight: PBS volume) and ultrasonically homogenized to prepare a homogenate. The resulting homogenous solution of 25 μL was diluted with 50 μL acetonitrile solution containing internal standard testosterone, vortexed, centrifuged at 12000 × g for 5 minutes, and collected the supernatant,then injected into LC-MS. The amount of payload MMAE in tissue was determined by LC-MS chromatogram equipped with a UV detector. The operation conditions of HPLC were the same as used in the calibration curve (gradient: 0.1-3.1 min, 5%-95% ACN, 3.1-5.0 min, 95% ACN, 5.0-5.5 min, 95%-5% ACN, 5.5-6.5 min, 5% ACN, 0.4 ml/min, equipped Phenomenex Kinetex® 2.6 μM F5 100 Å 50×2.1 mm column). The AUCs of each sample were obtained in triplicate. All animal tests were conducted in the Ethics Committee for Animal Experimentation of Greater Bay Area Institute of Precision Medicine (Guangzhou) in compliance with relevant laws and institutional rules.

Kiss-and-run experiment with conjugates P1 and P3

MDA-MB-231 (3.0×10^3 cells per well) and A549 cells (3.0×10^3 cells per well) were seeded in 96-well plates and incubated for 24 h. Then the medium was discarded and treated with **P1** or **P3** in various concentrations (40 μM, 20 μM, 10 μM, 5 μM, 2.5 μM, 1.25 μM, 0.625 μM, 0.3125 μM) for 1h at 37 ℃, followed by a washout of the treatment and a further incubation of the cells up to 72 h. Then a conventional CCK-8 treatment followed. After 1 h, the formazan dye was quantified using a microplate reader to assess absorbance at 450 nm (measurement wavelength) and 630 nm (reference wavelength). Non-treated cells were used as controls. The percentage viability of cells was estimated as the percentage fluorescence intensity in the experimental wells relative to that in the blank and negative control wells. Each experiment was repeated three times.

Data availability

Data generated during this study are included in the published article and in the supplemental information files supplied (Supplementary Data 1–3). All other datasets generated during this study are available from the corresponding authors upon reasonable request.

References

1 Rentero Rebollo, I. & Heinis, C. Phage selection of bicyclic peptides. *Methods* **60**, 46-54 (2013). https://doi.org:10.1016/j.ymeth.2012.12.008

2 Chung, B. K. & Yudin, A. K. Disulfide-bridged peptide macrobicycles from nature. *Org Biomol Chem* **13**, 8768-8779 (2015). https://doi.org:10.1039/c5ob01115a

3 Rhodes, C. A. & Pei, D. Bicyclic Peptides as Next-Generation Therapeutics. *Chemistry* **23**, 12690-12703 (2017). https://doi.org:10.1002/chem.201702117

4 Feng, D. *et al.* Current development of bicyclic peptides. *Chinese Chemical Letters* **34** (2023). https://doi.org:10.1016/j.cclet.2022.108026

5 Ullrich, S. & Nitsche, C. Bicyclic peptides: Paving the road for therapeutics of the future. *Peptide Science* **116** (2023). https://doi.org:10.1002/pep2.24326

6 Thombare, V. J. & Hutton, C. A. Bridged bicyclic peptides: Structure and function. *Peptide Science* **110** (2018). https://doi.org:10.1002/pep2.24057

7 Ahangarzadeh, S. *et al.* Bicyclic peptides: types, synthesis and applications. *Drug Discov Today* **24**, 1311-1319 (2019). https://doi.org:10.1016/j.drudis.2019.05.008

8 Heinis, C. & Winter, G. Encoded libraries of chemically modified peptides. *Curr Opin Chem Biol* **26**, 89-98 (2015). https://doi.org:10.1016/j.cbpa.2015.02.008

9 Danhier, F., Le Breton, A. & Preat, V. RGD-based strategies to target alpha(v) beta(3) integrin in cancer therapy and diagnosis. *Mol Pharm* **9**, 2961-2973 (2012). https://doi.org:10.1021/mp3002733

10 Bledzka, K., Smyth, S. S. & Plow, E. F. Integrin alphaIIbbeta3: from discovery to efficacious therapeutic target. *Circ Res* **112**, 1189-1200 (2013). https://doi.org:10.1161/CIRCRESAHA.112.300570

11 Gu, Y. *et al.* The challenges and opportunities of alphavbeta3-based therapeutics in cancer: From bench to clinical trials. *Pharmacol Res* **189**, 106694 (2023). https://doi.org:10.1016/j.phrs.2023.106694

12 He, S. *et al.* Enhanced Tumor Targeting and Penetration of Proteolysis-Targeting Chimeras through iRGD Peptide Conjugation: A Strategy for Precise Protein Degradation in Breast Cancer. *J Med Chem* **66**, 16828-16842 (2023). https://doi.org:10.1021/acs.jmedchem.3c01539

13 Zheng, J. *et al.* Bifunctional Compounds as Molecular Degraders for Integrin-Facilitated Targeted Protein Degradation. *J Am Chem Soc* **144**, 21831-21836 (2022). https://doi.org:10.1021/jacs.2c08367

14 Montenegro, C. F. *et al.* Blocking alphavbeta3 integrin by a recombinant RGD disintegrin impairs VEGF signaling in endothelial cells. *Biochimie* **94**, 1812-1820 (2012). https://doi.org:10.1016/j.biochi.2012.04.020

15 Liu, H. *et al.* The role of integrin alphavbeta3 in biphasic calcium phosphate ceramics mediated M2 Macrophage polarization and the resultant osteoinduction. *Biomaterials* **304**, 122406 (2024). https://doi.org:10.1016/j.biomaterials.2023.122406

16 Dechantsreiter, M. A. *et al.* N-Methylated cyclic RGD peptides as highly active and selective alpha(V)beta(3) integrin antagonists. *J Med Chem* **42**, 3033-3040 (1999). https://doi.org:10.1021/jm970832g

17 Mas-Moruno, C., Rechenmacher, F. & Kessler, H. Cilengitide: the first anti-angiogenic small molecule drug candidate design, synthesis and clinical evaluation. *Anticancer Agents Med Chem* **10**, 753-768 (2010). https://doi.org:10.2174/187152010794728639

18 Stupp, R. *et al.* Cilengitide combined with standard treatment for patients with newly diagnosed glioblastoma with methylated MGMT promoter (CENTRIC EORTC 26071-22072 study): a multicentre, randomised, open-label, phase 3 trial. *Lancet Oncol* **15**, 1100-1108 (2014). https://doi.org:10.1016/S1470-2045(14)70379-1

19 Nabors, L. B. *et al.* Two cilengitide regimens in combination with standard treatment for patients with newly diagnosed glioblastoma and unmethylated MGMT gene promoter: results of the open-label, controlled, randomized phase II CORE study. *Neuro Oncol* **17**, 708-717 (2015). https://doi.org:10.1093/neuonc/nou356

20 Kondo, N. *et al.* Radioiodinated Bicyclic RGD Peptide Derivatives for Enhanced Tumor Accumulation. *Pharmaceuticals* **18** (2025). https://doi.org:10.3390/ph18040549

21 Cheng, X., Li, C., Hong, H., Zhou, Z. & Wu, Z. Macrocyclic RGD-peptides with high selectivity for alpha(v)beta(3) integrin in cancer imaging and therapy. *RSC Med Chem* (2025). https://doi.org:10.1039/d5md00280j

22 Chen, H., Niu, G., Wu, H. & Chen, X. Clinical Application of Radiolabeled RGD Peptides for PET Imaging of Integrin alphavbeta3. *Theranostics* **6**, 78-92 (2016). https://doi.org:10.7150/thno.13242

23 Jin, Z. H. *et al.* Radiotheranostic Agent (64)Cu-cyclam-RAFT-c(-RGDfK-)(4) for Management of Peritoneal Metastasis in Ovarian Cancer. *Clin Cancer Res* **26**, 6230-6241 (2020). https://doi.org:10.1158/1078-0432.CCR-20-1205

24 Cossu, J., Thoreau, F. & Boturyn, D. Multimeric RGD-Based Strategies for Selective Drug Delivery to Tumor Tissues. *Pharmaceutics* **15** (2023). https://doi.org:10.3390/pharmaceutics15020525

25 Wen, X. *et al.* Synthesis, preclinical, and initial clinical evaluation of integrin alpha(V)beta(3) and gastrin-releasing peptide receptor (GRPR) dual-targeting radiotracer [(68)Ga]Ga-RGD-RM26-03. *Eur J Nucl Med Mol Imaging* **51**, 2023-2035 (2024). https://doi.org:10.1007/s00259-024-06634-9

26 Jin, Z. H. *et al.* Evaluation of the Gly-Phe-Lys Linker to Reduce the Renal Radioactivity of a [(64)Cu]Cu-Labeled Multimeric cRGD Peptide. *ACS Omega* **10**, 4102-4120 (2025). https://doi.org:10.1021/acsomega.4c10621

27 Xiao, L. & Xin, J. Advances in Clinical Oncology Research on (99m)Tc-3PRGD2 SPECT Imaging. *Front Oncol* **12**, 898764 (2022). https://doi.org:10.3389/fonc.2022.898764

28 Xiao, L., Yu, S., Xu, W., Sun, Y. & Xin, J. (99m)Tc-3PRGD(2) SPECT/CT Imaging for Diagnosing Lymph Node Metastasis of Primary Malignant Lung Tumors. *Korean J Radiol* **24**, 1142-1150 (2023). https://doi.org:10.3348/kjr.2023.0411

29 Huang, Y.-Q. *et al.* Design, synthesis and pharmacological evaluation of a novel PEG-cRGD-conjugated irinotecan derivative as potential antitumor agent. *European Journal of Medicinal Chemistry* **158**, 82-90 (2018). https://doi.org:10.1016/j.ejmech.2018.08.091

30 Lerchen, H.-G. *et al.* Discovery of VIP236, an αvβ3-Targeted Small-Molecule–Drug Conjugate with Neutrophil Elastase-Mediated Activation of 7-Ethyl Camptothecin Payload for Treatment of Solid Tumors. *Cancers* **15** (2023). https://doi.org:10.3390/cancers15174381

31 Kemker, I., Schnepel, C., Schroder, D. C., Marion, A. & Sewald, N. Cyclization of RGD Peptides by Suzuki-Miyaura Cross-Coupling. *J Med Chem* **62**, 7417-7430 (2019). https://doi.org:10.1021/acs.jmedchem.9b00360

32 Kemker, I. *et al.* Tuning the Biological Activity of RGD Peptides with Halotryptophans. *J Med Chem* **64**, 586-601 (2021). https://doi.org:10.1021/acs.jmedchem.0c01536

33 Wang, P. *et al.* Modular synthesis of clickable peptides via late-stage maleimidation on C(7)-H tryptophan. *Nat Commun* **14**, 3973 (2023). https://doi.org:10.1038/s41467-023-39703-y

34 Mitra, A. *et al.* Polymeric conjugates of mono- and bi-cyclic alphaVbeta3 binding peptides for tumor targeting. *J Control Release* **114**, 175-183 (2006). https://doi.org:10.1016/j.jconrel.2006.06.014

35 Koivunen, E., Wang, B. & Ruoslahti, E. Phage libraries displaying cyclic peptides with different ring sizes: ligand specificities of the RGD-directed integrins. *Biotechnology (N Y)* **13**, 265-270 (1995). https://doi.org:10.1038/nbt0395-265

36 Assa-Munt, N., Jia, X., Laakkonen, P. & Ruoslahti, E. Solution structures and integrin binding activities of an RGD peptide with two isomers. *Biochemistry* **40**, 2373-2378 (2001). https://doi.org:10.1021/bi002101f

37 Bogdanowich-Knipp, S. J., Chakrabarti, S., Williams, T. D., Dillman, R. K. & Siahaan, T. J. Solution stability of linear vs. cyclic RGD peptides. *J Pept Res* **53**, 530-541 (1999). https://doi.org:10.1034/j.1399-3011.1999.00052.x

38 Bernhagen, D. *et al.* Bicyclic RGD Peptides with Exquisite Selectivity for the Integrin alpha(v)beta(3) Receptor Using a "Random Design" Approach. *ACS Comb Sci* **21**, 198-206 (2019). https://doi.org:10.1021/acscombsci.8b00144

39 Timmerman, P., Beld, J., Puijk, W. C. & Meloen, R. H. Rapid and quantitative cyclization of multiple peptide loops onto synthetic scaffolds for structural mimicry of protein surfaces. *Chembiochem* **6**, 821-824 (2005). https://doi.org:10.1002/cbic.200400374

40 Kapp, T. G. *et al.* A Comprehensive Evaluation of the Activity and Selectivity Profile of Ligands for RGD-binding Integrins. *Sci Rep* **7**, 39805 (2017). https://doi.org:10.1038/srep39805

41 Yao, G. *et al.* Iodine-Mediated Tryptathionine Formation Facilitates the Synthesis of Amanitins. *J Am Chem Soc* **143**, 14322-14331 (2021). https://doi.org:10.1021/jacs.1c06565

42 Wieland, T. & Faulstich, H. Fifty years of amanitin. *Experientia* **47**, 1186-1193 (1991). https://doi.org:10.1007/BF01918382

43 Wu, C. *et al.* Novel N-Methylated Cyclodepsipeptide Prodrugs for Targeted Cancer Therapy. *J Med Chem* **64**, 991-1000 (2021). https://doi.org:10.1021/acs.jmedchem.0c01387

44 Chatzisideri, T. *et al.* Integrin-Mediated Targeted Cancer Therapy Using c(RGDyK)-Based Conjugates of Gemcitabine. *J Med Chem* **65**, 271-284 (2022). https://doi.org:10.1021/acs.jmedchem.1c01468

45 Liu, K. *et al.* Peptidic heterodimer-based radiotracer targeting fibroblast activation protein and integrin alpha(v)beta(3). *Eur J Nucl Med Mol Imaging* **51**, 1544-1557 (2024). https://doi.org:10.1007/s00259-024-06623-y

46 van den Kerkhof, D. L. *et al.* Unraveling the role of the homoarginine residue in antiplatelet drug eptifibatide in binding to the alphaIIbbeta3 integrin receptor. *Thromb Res* **217**, 96-103 (2022). https://doi.org:10.1016/j.thromres.2022.07.011

47 Tonin, G. & Klen, J. Eptifibatide, an Older Therapeutic Peptide with New Indications: From Clinical Pharmacology to Everyday Clinical Practice. *Int J Mol Sci* **24** (2023). https://doi.org:10.3390/ijms24065446

48 Frank, A. O. *et al.* Conformational control of integrin-subtype selectivity in isoDGR peptide motifs: a biological switch. *Angew Chem Int Ed Engl* **49**, 9278-9281 (2010). https://doi.org:10.1002/anie.201004363

49 Pfaff, M. e. a. Selective recognition of cyclic RGD peptides of NMR defined conformation by alpha IIb beta 3, alpha V beta 3, and alpha 5 beta 1 integrins. *J. Biol. Chem.* **269**, 20233–20238 (1994).

50 Weide, T., Modlinger, A. & Kessler, H. Spatial Screening for the Identification of the Bioactive Conformation of Integrin Ligands;. *Topics in Current Chemistry* **272**, 1-50 (2007). https://doi.org:10.1007/128_052

51 D'Mello V, C. *et al.* Characterization of Asx Turn Types and Their Connate Relationship with beta-Turns. *Chemistry* **28**, e202104328 (2022). https://doi.org:10.1002/chem.202104328

52 Newell, N. E. ExploreTurns: A web tool for the exploration, analysis, and classification of beta turns and structured loops in proteins; application to beta-bulge and Schellman loops, Asx helix caps, beta hairpins, and other hydrogen-bonded motifs. *Protein Sci* **34**, e70046 (2025). https://doi.org:10.1002/pro.70046

53 Chen, X., Plasencia, C., Hou, Y. & Neamati, N. Synthesis and biological evaluation of dimeric RGD peptide-paclitaxel conjugate as a model for integrin-targeted drug delivery. *J Med Chem* **48**, 1098-1106 (2005). https://doi.org:10.1021/jm049165z

54 Li, R. *et al.* Asymmetric, amphiphilic RGD conjugated phthalocyanine for targeted photodynamic therapy of triple negative breast cancer. *Signal Transduct Target Ther* **7**, 64 (2022). https://doi.org:10.1038/s41392-022-00906-2

55 DiCara, D. *et al.* Structure-function analysis of Arg-Gly-Asp helix motifs in alpha v beta 6 integrin ligands. *J Biol Chem* **282**, 9657-9665 (2007). https://doi.org:10.1074/jbc.M610461200

56 Park, S. H. *et al.* Development of a Peptide-Based Nano-Sized Cathepsin B Inhibitor for Anticancer Therapy. *Pharmaceutics* **15** (2023). https://doi.org:10.3390/pharmaceutics15041131

57 Li, H. *et al.* Cathepsin B-Activated PET Tracer for In Vivo Tumor Imaging. *Mol Pharm* **21**, 1382-1389 (2024). https://doi.org:10.1021/acs.molpharmaceut.3c01034

58 Liu, F. *et al.* Cathepsin B: The dawn of tumor therapy. *Eur J Med Chem* **269**, 116329 (2024). https://doi.org:10.1016/j.ejmech.2024.116329

59 Raposo Moreira Dias, A. *et al.* Synthesis and Biological Evaluation of RGD and isoDGR-Monomethyl Auristatin Conjugates Targeting Integrin alpha(V) beta(3). *ChemMedChem* **14**, 938-942 (2019). https://doi.org:10.1002/cmdc.201900049

60 Akaiwa, M., Dugal-Tessier, J. & Mendelsohn, B. A. Antibody-Drug Conjugate Payloads; Study of Auristatin Derivatives. *Chem Pharm Bull (Tokyo)* **68**, 201-211 (2020). https://doi.org:10.1248/cpb.c19-00853

61 Feni, L. *et al.* Kiss and Run: Promoting Effective and Targeted Cellular Uptake of a Drug Delivery Vehicle Composed of an Integrin-Targeting Diketopiperazine Peptidomimetic and a Cell-Penetrating Peptide. *Bioconjugate Chemistry* **30**, 2011-2022 (2019). https://doi.org:10.1021/acs.bioconjchem.9b00292

62 Zambra, M. *et al.* Optimizing the enzymatic release of MMAE from isoDGR-based small molecule drug conjugate by incorporation of a GPLG-PABC enzymatically cleavable linker. *Frontiers in Pharmacology* **14** (2023). https://doi.org:10.3389/fphar.2023.1215694

63 Colombo, R. *et al.* Synthesis and biological evaluation (in vitro and in vivo) of cyclic arginine-glycine-aspartate (RGD) peptidomimetic-paclitaxel conjugates targeting integrin alphaVbeta3. *J Med Chem* **55**, 10460-10474 (2012). https://doi.org:10.1021/jm301058f

Acknowledgments

This work was supported by the National Natural Science Foundation of China (grants 82204189) and Guangdong Basic and Applied Basic Research Foundation (2022A1515111207).

Author Contributions

#H.Y., H.P. and T. R. contributed equally to this work. H.Y. synthesized the target compounds, completed HPLC analysis and performed partial biological assays. H.P., W.D. and J.T. completed most biological assays and analyzed part of the data. W.P. performed the pharmacokinetic experiments. T. R. performed the theoretical calculations and molecular docking. G.Y., W.S., R.D.S. and J.S. proposed the project. G.Y., R.D.S. and H.Y. performed data analysis and contributed to the writing-review and editing of the manuscript. All authors have given approval to the final version of the manuscript.

Competing interests

The authors declare no competing interests.

Supplementary materials

Supplementary material associated with this article can be found, in the online version, at xxxx

Figure legends

Figure 1. Reported structures of bicyclic peptides targeting αvβ3: a) RGD4C and b) CLIPS peptide CT3HPQcT3RGDcT3. c) Design strategy of bicyclic peptides in this study; R* corresponds to Arg, *nor*Arg, and *homo*Arg; $G^{\#}$ corresponds to Gly, βAla and GABA.

Figure 2. Impact of the sidechain guanidine on integrin selectivity. a) Chemical structures of **5d**, **5i**, **5j, 6** *c*(RGDyK)**, 7** (Eptifibatide). b) IC_{50} values and selectivity of peptides with various Arg-homologs (**5d**, **5i**, **5j**, **6** and **7**) for integrin αvβ3 and αIIbβ3 (ratio[a] =αIIbβ3: αvβ3). c-d) MD simulations and molecular docking of the binding mode of peptide **5j** with c) αvβ3 (PDB: 1L5G) and d) αIIbβ3 (PDB: 8T2U) integrin. Stick model: compound **5j** (deep pink), protein side chains of the integrin binding pocket (green sticks, with their secondary structures illustrated as a cartoon). The interactions were visualized using ChimeraX.

Figure 3. Binding and internalization of Cy5-labeled peptides in αvβ3-expressing cell. a) Expression of integrin αvβ3 and αvβ6 in MDA-MB-231 (αvβ3+, αvβ6-), A549 (αvβ3+, αvβ6-) and Huh-7 (αvβ3-, αvβ6-) cells. b) Cell binding assay. MDA-MB-231 and Huh-7 cells were incubated with 5 μM of Cy5-labeled peptides (at 4 ℃ for 1 h). Cells were washed, fixed, labeled with DAPI, and imaged with confocal microscopy. c). Cellular uptake and co-localization of Cy5-labeled peptides with lysosomes in MDA-MB-231 cells. d-e) Co-localization curve of Cy5-labeled peptides with lysosome marker. Cells were pretreated with 5 μM Cy5-labeled peptides for 4 h, then fixed, labeled with DAPI and LAMP1. Fluorescence signals indicating the colocalization of Cy5-labeled peptide (red) with the lysosome marker (LysoTracker, green) in MDA-MB-231 cells (blue is the nucleus, green is the lysosome, and red is the fluorescence of Cy5, the scale is 10 μm).

Figure 4. *In vivo* antitumor activity and safety profile of peptide-drug conjugates. a) Chemical structures of **P1**, **P2**, **P3, P4**. b-e) A549 tumor-bearing mice (n = 7) were injected intravenously with 1.0 mg kg-1 **P1** and 0.29 mg kg^{-1} MMAE every two days for three weeks. PBS was used as a vehicle. Tumor volumes and body weight were recorded. f) Liver and kidney functions were evaluated at the end of the treatment. g) Representative images of Ki67 staining of tumor sections in different groups. Bar = 50 μm. Statistical significances were analyzed by one-way ANOVA with Tukey's multiple comparisons test. All the data were plotted as mean ± SD. (*): $p < 0.05$, (***): $p < 0.001$.

Scheme 1. Synthesis and reaction conditions of a bicyclic octapeptide library: Fmoc-AA$_{1\text{-}n}$-OH can stand for Fmoc-Pro-OH, Fmoc-Ala-OH, Fmoc-Asn(Trt)-OH, Fmoc-Trp-OH, Fmoc-Asp(OtBu)-OH, Fmoc-Cys(Trt)-OH, Fmoc-*homo*Cys(Trt)-OH or Fmoc-D-Cys(Trt)-OH, R* or G$^{\#}$; R* is Fmoc-Arg(Pbf)-OH, Fmoc-*homo*Arg(Pbf)-OH or Fmoc-*nor*Arg(Pbf)-OH; G$^{\#}$ is Fmoc-Gly-OH, Fmoc-β-Ala-OH or Fmoc-GABA-OH; (a) 20% piperidine in DMF for 10 min (twice); (b) Fmoc-AA-OH (4.0 eq.), TBTU (4.0 eq.), DIEA (12.0 eq.), DMF, 1h; (c) 2 mg/ml I_2 in DMF, N_2, 2 h; (d) HFIP:DCM (3:7), 10 ml, r.t., 2 h; (e) HATU (2.0 eq.), DIEA (2.2 eq.), 0 °C to r.t., 12 h; (f) TFA:TIPS:H_2O (95:2.5:2.5), 30 min.

Table 1. Inhibition constants for synthetic peptides against the integrin subtypes αvβ3, αvβ5, αvβ6, αvβ8, α5β1, and αIIbβ3, (competitive ELISA; see Methods). 3-MPA is 3-mercaptopropionic acid, GABA is γ-aminobutyric acid. Reference compounds are *c*(RGDyK) **6** and Eptifibatide **7**[40].

Number	Compounds	IC$_{50}$ (nM)					
		α5β1	**αvβ3**	**αvβ5**	**αvβ6**	**αIIbβ3**	**αvβ8**
6	***c*(RGDyK)**	502 ± 203	1.4 ± 0.8	11.1± 4.3	136± 73	615 ± 490	216 ± 6.0
5a		361 ± 5.4	<0.51	13.2 ± 1.2	224 ± 88	1.9 ± 0.3	>1000
5b		958 ± 64	7.8 ± 0.4	113 ± 19	30.4 ± 16	5.7 ± 1.7	>1000
5c		127 ± 14	0.2 ± 0.002	25.3 ± 1.0	14.1± 4.5	0.2 ± 0.04	438± 118
5d		164 ± 3.0	<0.51	5.9 ± 0.3	36.7 ± 14.7	7.3 ± 3.4	143 ± 52
5e	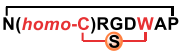	947 ± 30.6	4.9 ± 0.4	126 ± 23.7	37.5 ± 22.6	9.0 ± 1.1	30.3 ± 27.4
5f	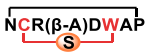	>1000	25.8 ± 2.6	>1000	>1000	>1000	>1000
5g	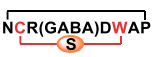	>1000	234 ± 15	>1000	>1000	16.4 ± 4.4	>1000

5h		57.8 ± 29.1	2.9 ± 0.2	19.0 ± 2.7	131 ± 46	86.5 ± 42.9	244 ± 87.3
5i	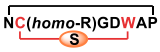	>1000	45.2 ± 8.3	718 ± 198	>1000	16.7 ± 0.1	>1000
5j	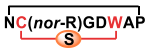	80.0 ± 23.1	0.7 ± 0.1	8.6 ± 1.3	111 ± 10.6	164 ± 24.0	496 ± 103
5k		121 ± 0.7	0.3 ± 0.003	2.2 ± 0.2	165 ± 7.7	2.9 ± 0.4	451 ± 243
7	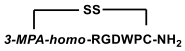	>1000	>1000	>1000	>1000	2.4 ± 0.5	>1000

Table2. Cytotoxicity of peptide **5j-K**, **6** *c*(RGDyK), free MMAE, **P1**, **P2, P3** and **P4** in αvβ3 positive cell lines MDA-MB-231 and A549.

Compounds	**IC_{50} (nM)**	
	MDA-MB-231	**A549**
5j-K	>5000	>5000
P1 (5j-PEG_8-VA-MMAE)	41.3 ± 4.1	28.9 ± 4.6
P2 (5j-C_8-VA-MMAE)	31.3 ± 4.3	18.5 ± 4.0
P3 (8-PEG_8-VA-MMAE)	72.2 ± 7.9	94.1 ± 25.9
6 [*c*(RGDyK)]	>5000	>5000
P4 (6-PEG_8-VA-MMAE)	58.5 ± 3.9	37.9 ± 8.4
MMAE	<1.37	<1.37

Table 3. In vitro cytotoxicity of compounds **P1**, **P2**, **P4** and MMAE against A549-si-NC (αvβ3+) and A549-KD (αvβ3-) cells.

Compounds	IC_{50} (nM)	
	A549-si-NC (αvβ3+)	A549-KD (αvβ3-)
P1 (5j-PEG_8-VA-MMAE)	10.9 ± 1.4	17.0 ± 0.6
P2 (5j-C_8-VA-MMAE)	5.2 ± 0.1	10.0 ± 1.9
P4 (6-PEG_8-VA-MMAE)	10.5 ± 1.7	18.4 ± 3.5
MMAE	<0.15	<0.15

Editor's Summary

Bicyclic peptides targeting integrin are promising drug candidates, yet achieving high selectivity for specific integrins remains challenging. Here, the authors design RGD-containing bicyclic peptides with a tryptathionine bridge, demonstrating that peptide 5j selectively targets integrin αvβ3, and induces αvβ3-targeted cytotoxicity by drug-peptide conjugates.

Peer review information:
Communications Chemistry thanks Didier Boturyn and the other, anonymous, reviewer(s) for their contribution to the peer review of this work.

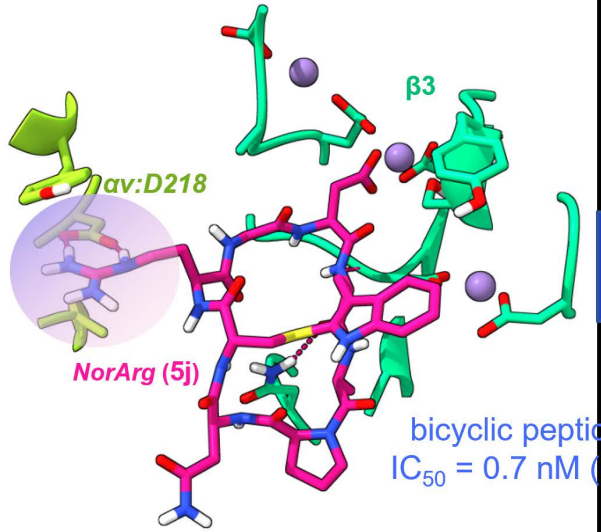

bicyclic peptide **5j**
IC_{50} = 0.7 nM (αvβ3)

Peptide Drug Conjugate (P1)

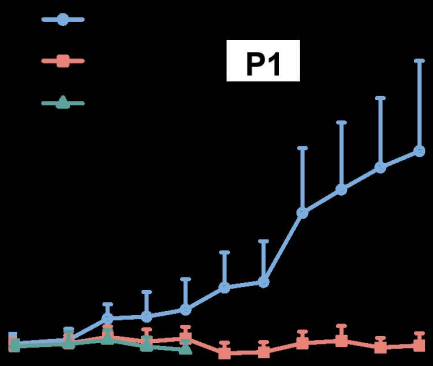

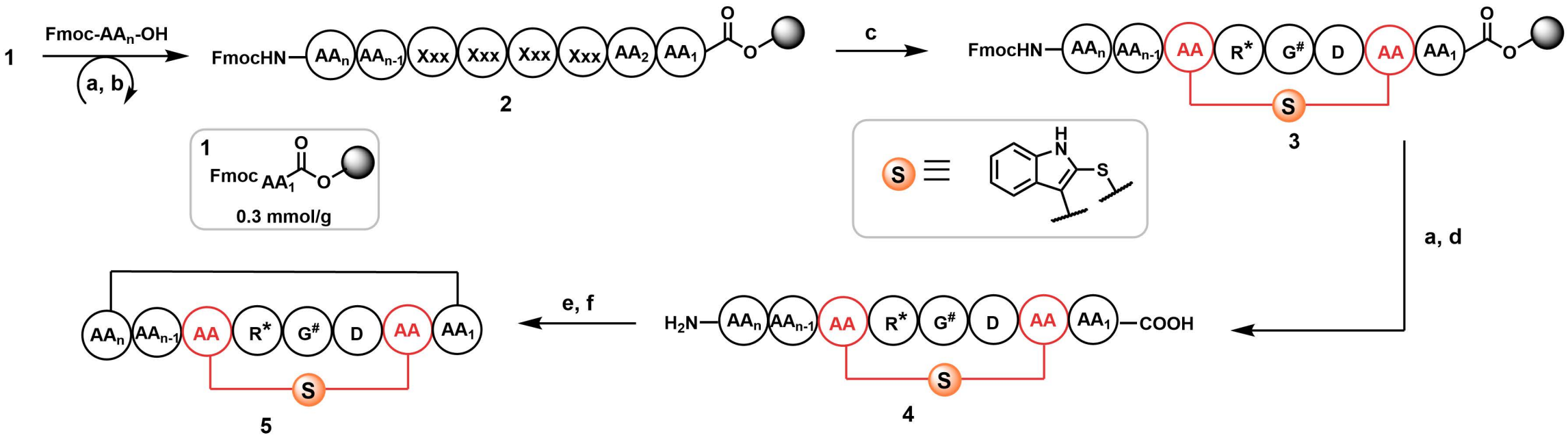
1
Fmoc-AAn-OH
a, b
FmocHN
AAn
AAn-1
Xxx
Xxx
Xxx
Xxx
AA2
AA1
O
2
c
FmocHN
AAn
AAn-1
AA
R*
G#
D
AA
AA1
S
3
1
Fmoc
AA1
0.3 mmol/g
S
H
N
S
a, d
H2N
AAn
AAn-1
AA
R*
G#
D
AA
AA1
COOH
S
4
e, f
AAn
AAn-1
AA
R*
G#
D
AA
AA1
S
5

a) Ruoslahti et al. (1995)

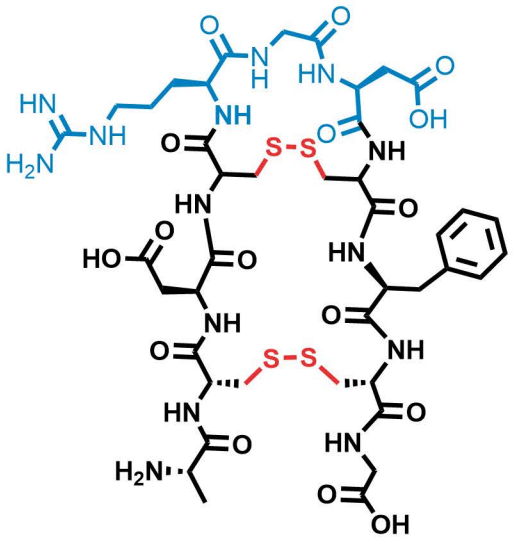

RGD4C, (RGD)

IC_{50} = 8.3 ± 2.1 nM (αvβ3)

b) Bernhagen et al. (2019)

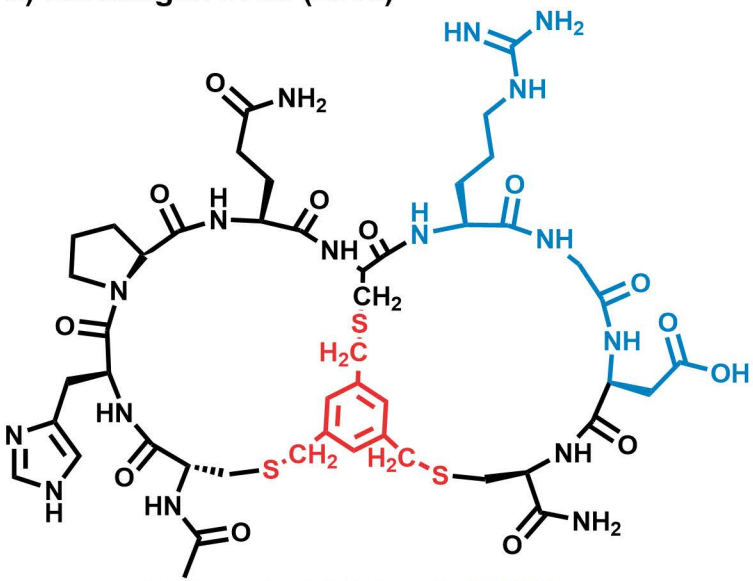

CT3HPQcT3RGDcT3 (RGD)

IC_{50} = 30 ± 4 nM (αvβ3)

c) This Work

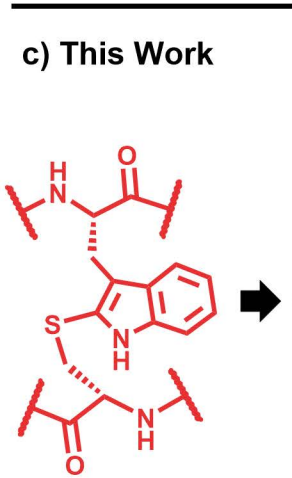

tryptathionine

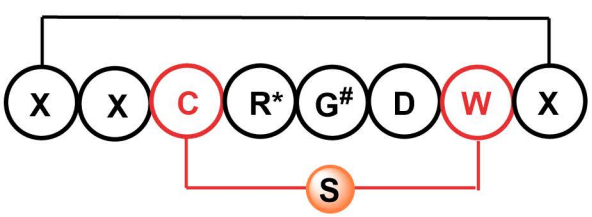

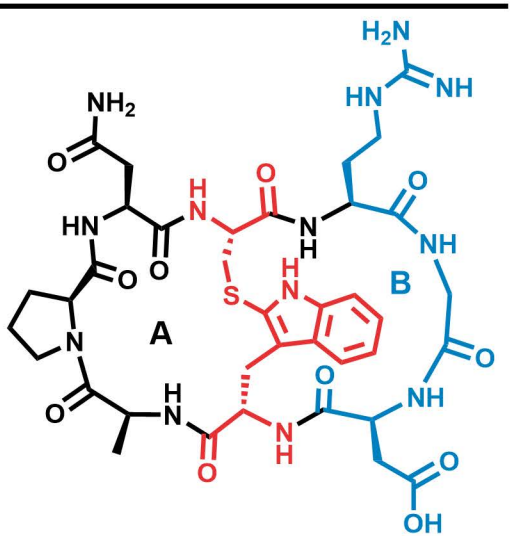

bicyclic peptide 5j (*nor*RGD)

IC_{50} = 0.7 ± 0.1 nM (αvβ3)

√ ***High binding affinity*** √ ***Atypical sequence*** √ ***Constrained conformation***

a)

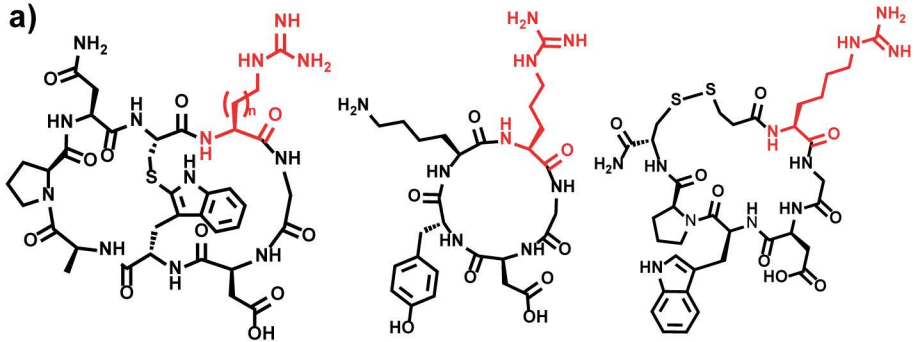

5d, 5i and 5j

6. c(RGDyK)

7. Eptifibatide

b)

Number	Arg mutation	IC$_{50}$(nM) αvβ3	IC$_{50}$(nM) αIIbβ3	ratio[a]
6	Arg	1.4	615	430
7	*homo* Arg	>1000	2.4	/
5j	*nor* Arg	0.7	164	234
5d	Arg	<0.51	7.3	/
5i	*homo* Arg	45.2	16.7	0.37

c)

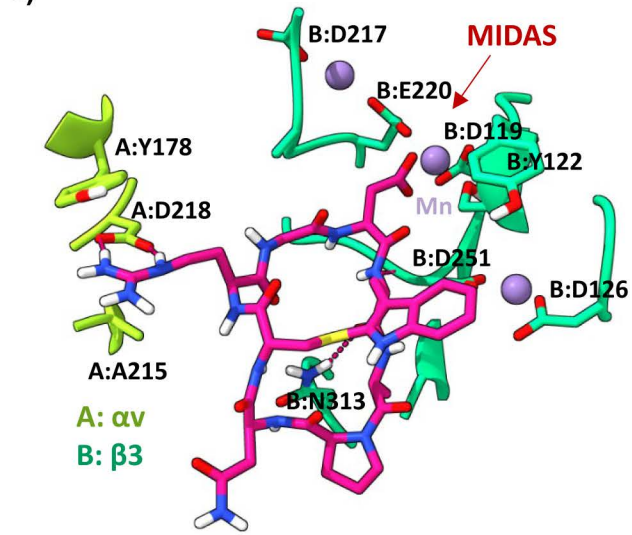

d)

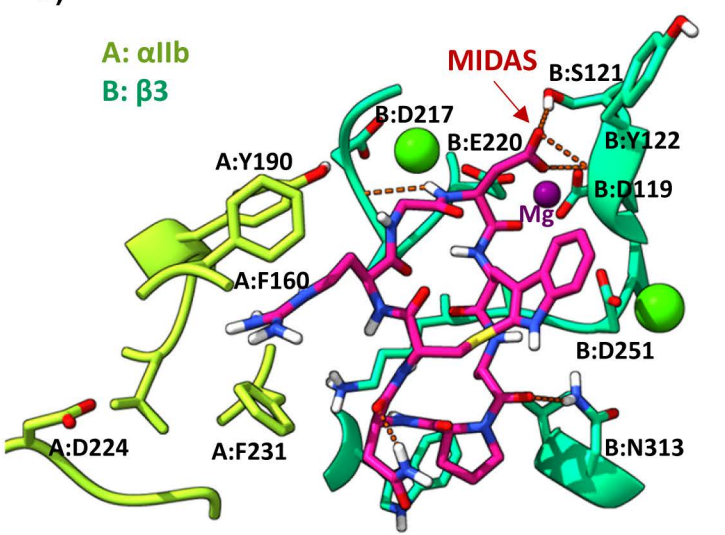

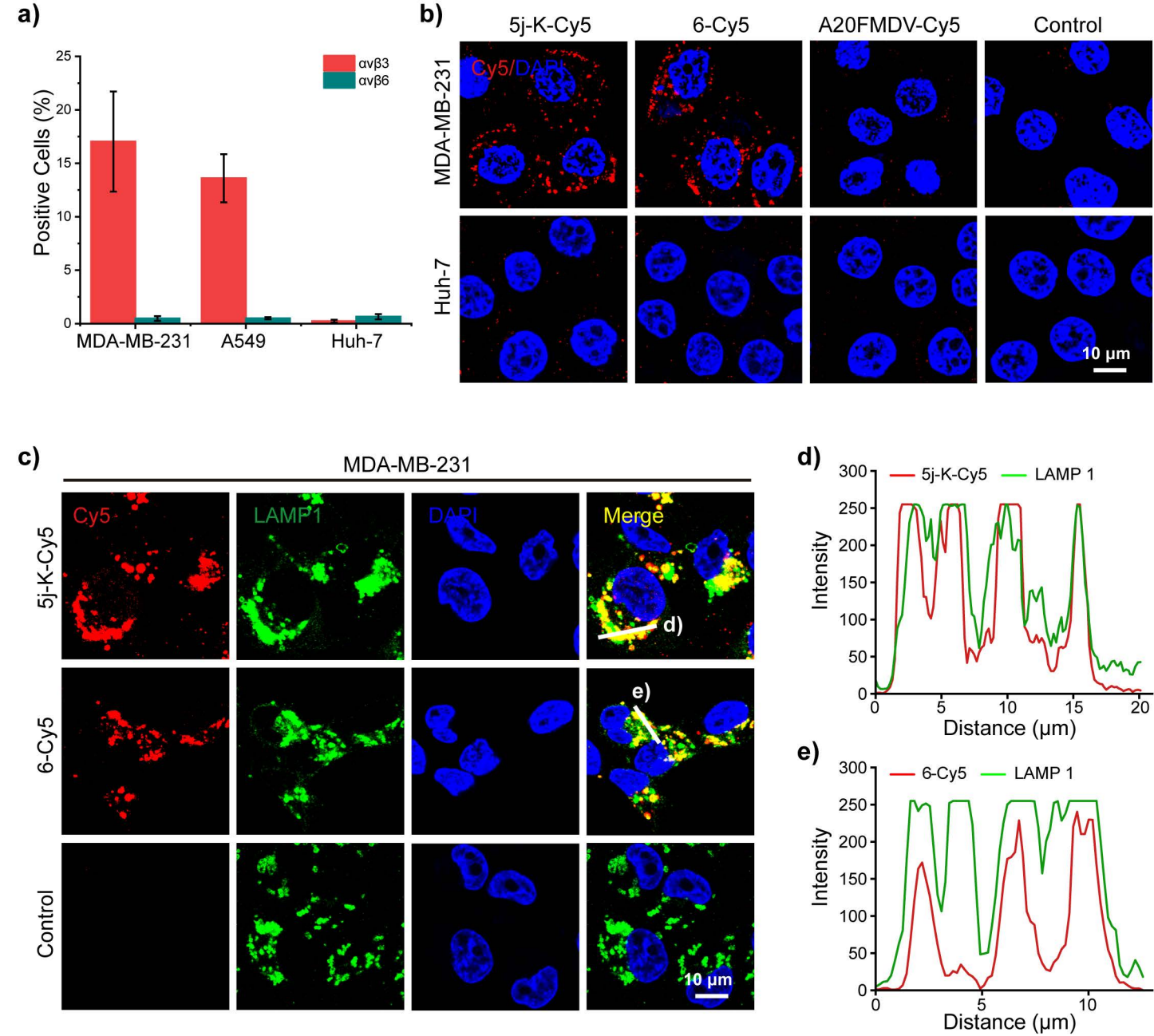
a)
Positive Cells (%)
αvβ3
αvβ6
MDA-MB-231
A549
Huh-7
b)
5j-K-Cy5
6-Cy5
A20FMDV-Cy5
Control
MDA-MB-231
Huh-7
Cy5/DAPI
10 μm
c)
MDA-MB-231
Cy5
LAMP1
DAPI
Merge
5j-K-Cy5
6-Cy5
Control
d)
e)
10 μm
d)
5j-K-Cy5
LAMP 1
Intensity
Distance (μm)
e)
6-Cy5
LAMP 1
Intensity
Distance (μm)

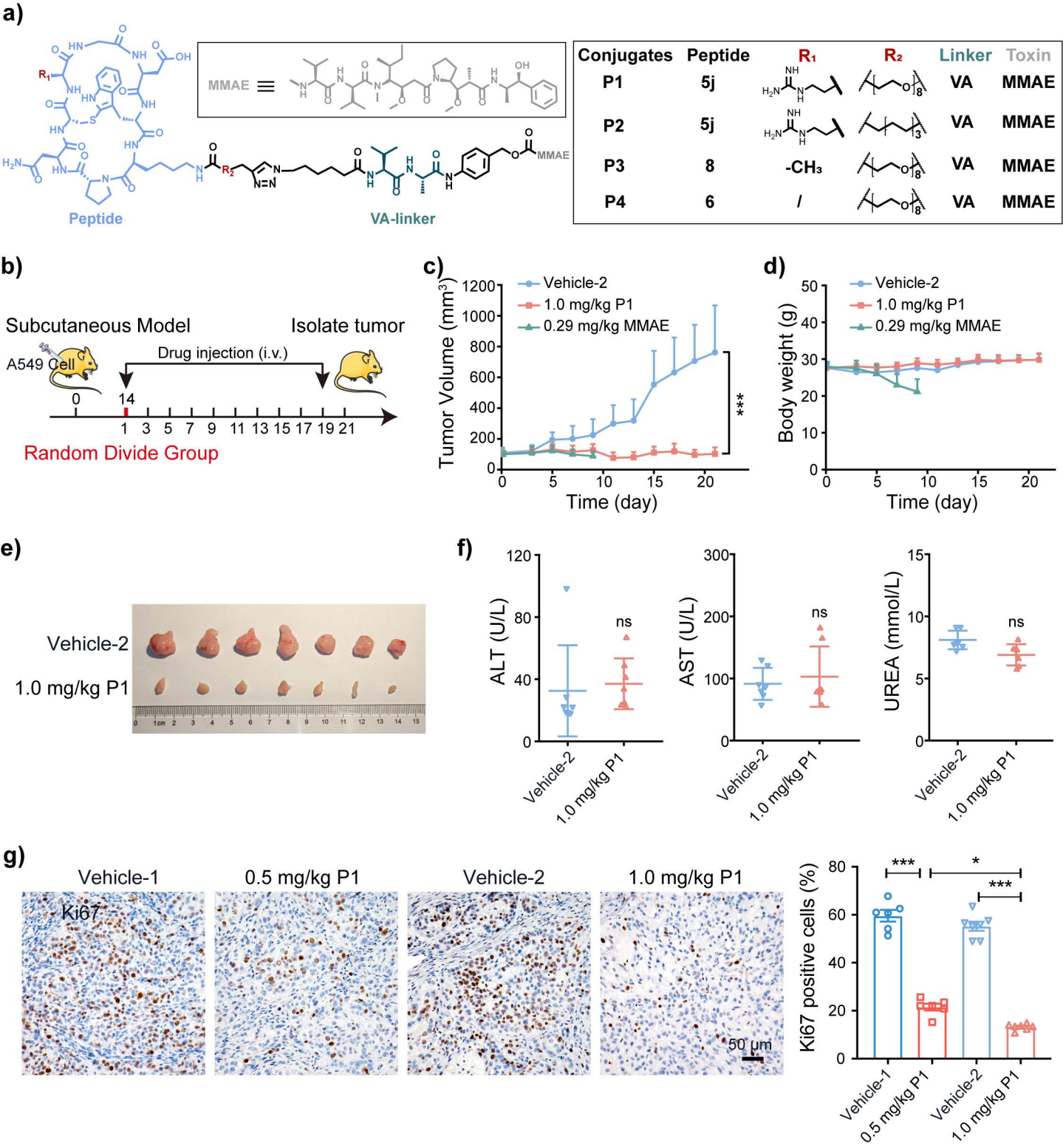
a)
MMAE
Peptide
VA-linker
Conjugates Peptide R1 R2 Linker Toxin
P1 5j VA MMAE
P2 5j VA MMAE
P3 8 -CH3 VA MMAE
P4 6 / VA MMAE
b)
Subcutaneous Model
Isolate tumor
A549 Cell
Drug injection (i.v.)
0 14
1 3 5 7 9 11 13 15 17 19 21
Random Divide Group
c)
Vehicle-2
1.0 mg/kg P1
0.29 mg/kg MMAE
Tumor Volume (mm3)
Time (day)
***
d)
Vehicle-2
1.0 mg/kg P1
0.29 mg/kg MMAE
Body weight (g)
Time (day)
e)
Vehicle-2
1.0 mg/kg P1
f)
ALT (U/L)
AST (U/L)
UREA (mmol/L)
ns
Vehicle-2
1.0 mg/kg P1
g)
Vehicle-1
0.5 mg/kg P1
Vehicle-2
1.0 mg/kg P1
Ki67
50 μm
Ki67 positive cells (%)
***
*
***
Vehicle-1
0.5 mg/kg P1
Vehicle-2
1.0 mg/kg P1